Reaction Fields in the Environment of Fluorescent Probes: Polarity Profiles in Membranes

Derek Marsh*
Max-Planck-Institut für biophysikalische Chemie, Abteilung Spektroskopie, Göttingen, Germany

ABSTRACT Fluorescent probes in biological systems are sensitive to environmental polarity by virtue of their response to the reaction field created by polarization of the dielectric medium. Classically, fluorophore solvatochromism is analyzed in terms of the Lippert equation and later variants, all of which rely upon the original reaction field of Onsager. A recent survey of the solvent dependence of EPR spin-label probes, which are responsive solely to the reaction field in the ground state without the complication of excited states, shows that the reaction field of Block and Walker performs best in describing the polarity dependence. In this model, the step-function transition to the bulk dielectric medium used by Onsager is replaced by a graded transition. Analysis of the Stokes shifts for representative fluorescent membrane probes, such as PRODAN, DANSYL, and anthroyl fatty acid, reveals that, of several different reaction fields (including that of Onsager), the Block-Walker model best describes the dependence on solvent dielectric constant and refractive index for the different probes simultaneously. This is after full allowance is made for all contributions involving polarizability of the fluorophore, a point that is frequently neglected or treated incorrectly in studies using biological fluorescent probes. By using the full range of polar and apolar solvents, it is then possible to establish a common reference for the polarity dependence of different fluorophores and to relate this also to the polarity dependence of biologically relevant spin-label EPR probes. An important application is calibration of the transmembrane polarity profile recorded by fluorescent probes in terms of the high-resolution profile obtained from site-specifically spin-labeled lipid chains.

INTRODUCTION

The polarity profile across biological membranes determines the permeability barrier, partition coefficients of solutes, and the energetics and stability of protein insertion. For lipid membranes, the transmembrane profiles are best determined by nitroxide spin-label electron paramagnetic resonance (EPR) (1–5). Fluorescent lipid probes such as anthroyl fatty acids and LAURDAN (see Fig. 1) lack, in general, the positional precision of spin-labeled lipids, although they may be used to probe less local regional polarity (6–8). On the other hand, AEDANS [*N*-(iodoacetylaminoethyl)-5-naphthylamine-1-sulphonic acid] fluorescent labels have been used with considerable success to determine the transmembrane polarity profiles sensed by bitopic membrane proteins (9). More recently, fluorescence maxima from site-specific tryptophan mutants have also been used to determine the polarity profile for transmembrane segments of the mechano-sensitive ion channel, MscL (10). A quantitative comparison of the polarities sensed by the different classes of probes can best be achieved by calibrations with solvents of different polarities.

The polarity sensitivity of both spin-labeled and fluorescent biological probes arises from the reaction field of the solvents (11,12). This forms a common basis for transfer between the different data sets on polarity dependence. Whereas different reaction fields have been used for the analysis of the solvent dependence of EPR spectra from spin-label probes (2,13–18), solvent-dependent shifts in absorption and fluorescence spectra have almost invariably been interpreted in terms of the original Onsager reaction field (19–26).

Recently, the performance of different reaction fields has been compared for a range of biophysically used nitroxide spin-label probes in homogeneous solvents (27). It was concluded that the modification of the Onsager reaction field proposed by Block and Walker (28) was best able to describe the solvent dependence of the EPR spectra, when a realistic value was assumed for the polarizability of the nitroxide. Such a systematic comparison of different reaction fields has so far not been made for the solvent dependence of biologically relevant fluorescent probes. The EPR measurements are confined to the ground state of the spin label and therefore afford a more straightforward test of the different reaction fields than do optical spectra, which additionally involve excited states and nonequilibrium Franck-Condon states.

The purpose of this article is to compare the performance of the different reaction fields for characterizing the solvent dependence of fluorescent probes and to relate this to biophysical studies. The reaction field forms the basis for transferring the polarity dependences between different fluorescent probes, and between fluorescent probes and spin probes. The latter is particularly important in the case of membranes, and applications in this area are illustrated.

POLARITY DEPENDENCE OF OPTICAL SPECTRA

The original derivation of the solvent dependence of the Stokes shift for fluorescent probes was by Lippert (20,29), and used the Onsager reaction field without allowance for

Submitted August 25, 2008, and accepted for publication January 5, 2009.

*Correspondence: dmarsh@gwdg.de

Editor: Edward H. Egelman.

0006-3495/09/04/2549/10 $2.00

doi: 10.1016/j.bpj.2009.01.006

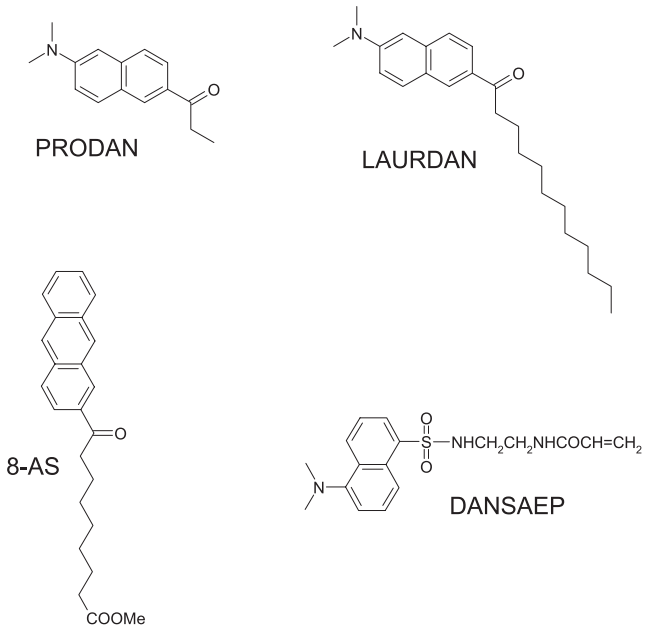

FIGURE 1 Chemical structures of polarity-sensitive fluorescent probes.

the polarizability of the fluorophore. Subsequently, it was recognized that the polarizability could make significant contributions to solvent-dependent shifts of both absorption and emission spectra (21–25). Unfortunately, the various treatments led to somewhat different results, as is clear from the summary that was given recently by Kawski (26). The origins of these discrepancies were analyzed in detail by Liptay (25); they correspond to neglect of one or another contribution to the energy of the chromophore in its reaction field. Notably, energy contributions from polarization either of the dielectric, or of the chromophore, have been neglected. The result is that some expressions derived for the shift in absorption or emission frequency are incorrect, even in the absence of polarizability of the chromophore. The amendment that is made in the recent edition of a well-respected textbook (30), which is much quoted in the biological field, is itself incorrect.

The treatment given here follows that of Liptay (25), although it is less general. In the absence of polarizability of the chromophore, the results from classical electrostatics that are given by Lippert (29) agree fully with those of Liptay (25).

Reaction field and energy in the ground state

The total electric dipole moment of the chromophore in the ground state is given by

$$\mathbf{m}_g = \mathbf{p}_g + \alpha_g \mathbf{R}_g, \tag{1}$$

where $\mathbf{p}_g$ and α_g are the permanent dipole moment and polarizability of the chromophore in the ground state. $\mathbf{R}_g$ is the reaction field at the chromophore that results from polarization of the dielectric environment by the dipole moment $(\mathbf{m}_g)$ of the chromophore. Consequently, the reaction field may be expressed in the form (31,32)

$$\mathbf{R}_g = f\mathbf{m}_g \equiv f(\varepsilon_r)\frac{\mathbf{m}_g}{4\pi\varepsilon_o r_{eff}^3}, \tag{2}$$

where ε_o is the permittivity of free space, ε_r is the relative dielectric permittivity of the solvent, and r_{eff} is an effective molecular interaction radius of the chromophore. From Eqs. 1 and 2, the reaction field, allowing for polarizability of the chromophore, is

$$\mathbf{R}_g = \frac{f}{1-\alpha_g f}\mathbf{p}_g \tag{3}$$

in the ground state. Then, from Eqs. 1 and 3, the total dipole moment in the ground state is

$$\mathbf{m}_g = \frac{\mathbf{p}_g}{1-\alpha_g f}. \tag{4}$$

The energy of the chromophore dipole, $\mathbf{p}_g$, in its own reaction field is given by (32)

$$W_g = -\frac{1}{2}\mathbf{p}_g \cdot \mathbf{R}_g. \tag{5}$$

Hence, from Eq. 3,

$$W_g = -\frac{1}{2}\frac{f}{1-\alpha_g f}|\mathbf{p}_g|^2 \tag{6}$$

in the ground state. This expression includes both the work done in polarizing the dielectric and the energy of the chromophore dipole in the reaction field (see (25)).

Reaction field and dipole moment in the Franck-Condon excited state

In analogy to Eq. 1, the local electric dipole moment in the excited state is given by

$$\mathbf{m}_e = \mathbf{p}_e + \alpha_e \mathbf{R}_e^{FC}, \tag{7}$$

where $\mathbf{p}_e$ and α_e are the dipole moment and polarizability of the chromophore in the exited state. $\mathbf{R}_e^{FC}$ is the reaction field in the Franck-Condon excited state, immediately after absorption of the radiation (see Fig. 2). The electronic polarization of the solvent responds immediately to the increased dipole moment of the chromophore, $\mathbf{p}_e$, in the excited state. This immediate response is characterized by a relative dielectric permittivity $\varepsilon_\infty = n^2$ where n is the refractive index of the solvent. The electronic component of the reaction field is induced by the total moment, $\mathbf{m}_e$, of the chromophore and is therefore given by (compare to Eq. 2)

$$R_e^{el} = f'\mathbf{m}_e \equiv f(n^2)\frac{\mathbf{m}_e}{4\pi\varepsilon_o r_{eff}^3}. \tag{8}$$

(Note that the functions $f(\ldots)$ have the same functional forms in Eqs. 2 and 8.) The polarization of the permanent dipoles in

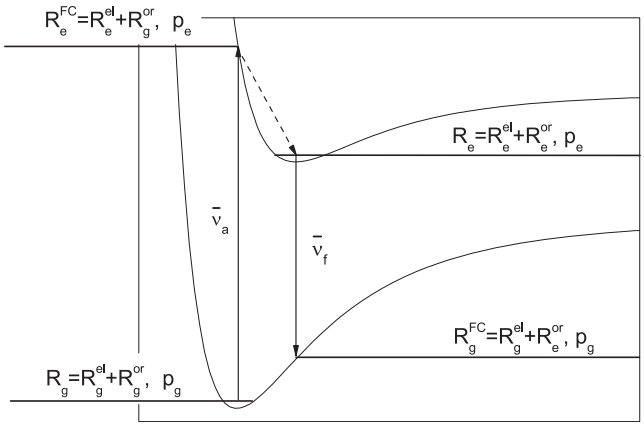

FIGURE 2 Reaction fields, R, and dipole moments, p, in the ground (g) and excited (e) states. $\bar{\nu}_a$ and $\bar{\nu}_f$ are the absorption and fluorescence transitions, respectively. Superscript FC indicates the Franck-Condon state. Thin lines indicate the potential surfaces in the ground (S_o) and first excited (S_1) singlet states. Superscripts el and or indicate the electronic and orientational contributions of the dielectric to the reaction field, respectively.

the solvent reorients only slowly (with the characteristic dielectric relaxation time, τ_D), relative to the time required for absorption of the radiation (~10^{-15}s). Therefore, the orientational component of the reaction field in the Franck-Condon excited state is equal to that in the ground state, $\mathbf{R}_g^{or}$. From Eqs. 7 and 8, with $\mathbf{R}_e^{FC} = \mathbf{R}_e^{el} + \mathbf{R}_g^{or}$, the electronic component of the reaction field in the Franck-Condon excited state is then given by

$$\mathbf{R}_e^{el} = \frac{f'}{1-\alpha_e f'}(\mathbf{p}_e + \alpha_e \mathbf{R}_g^{or}). \tag{9}$$

Correspondingly, the total reaction field is given by

$$\mathbf{R}_e^{FC} = \mathbf{R}_e^{el} + \mathbf{R}_g^{or} = \frac{f'\mathbf{p}_e + \mathbf{R}_g^{or}}{1-\alpha_e f'}. \tag{10}$$

Equations 9 and 10 both require knowledge of $\mathbf{R}_g^{or}$.

The orientational component of the reaction field in the ground state is given by the difference between the total reaction field, $\mathbf{R}_g$, and the electronic component of the reaction field, $\mathbf{R}_g^{el}$. Analogous to Eq. 8, the latter is given by $\mathbf{R}_g^{el} = f'\mathbf{m}_g$. Hence, the orientational component of the reaction field in the ground state (and in the Franck-Condon excited state) is given by

$$\mathbf{R}_g^{or} = \mathbf{R}_g - f'\mathbf{m}_g = \frac{f-f'}{1-\alpha_g f}\mathbf{p}_g, \tag{11}$$

where use has been made of Eqs. 3 and 4.

Returning to the Franck-Condon excited state, the total reaction field is finally given by

$$\mathbf{R}_e^{FC} = \frac{1}{1-\alpha_e f'}\left(f'\mathbf{p}_e + \frac{f-f'}{1-\alpha_g f}\mathbf{p}_g\right), \tag{12}$$

where use is made of Eqs. 10 and 11. From Eqs. 7 and 12, the total dipole moment of the fluorophore becomes

$$\mathbf{m}_e = \frac{1}{1-\alpha_e f'}\left(\mathbf{p}_e + \frac{\alpha_e(f-f')}{1-\alpha_g f}\mathbf{p}_g\right) \tag{13}$$

in the Franck-Condon excited state.

Energy in the Franck-Condon excited state and the absorption spectrum

Because the Franck-Condon state, unlike the ground state, is not an equilibrium state, it is not possible to use an analog of Eq. 5 for the total energy of the dipole in the excited state. As pointed out by Liptay (25), it is necessary to consider the work done in polarizing the dielectric ($+\frac{1}{2}\mathbf{m}\cdot\mathbf{R}$) and the energy of the dipole in the reaction field ($-\mathbf{p}\cdot\mathbf{R} - \frac{1}{2}\alpha^2 R^2$) separately. (Note: the validity and completeness of this method of calculation is demonstrated by applying the same approach to calculate the ground-state energy. This agrees with the classic result from equilibrium electrostatics (32), viz. Eq. 5; see (25).) Making the distinction between the orientational and electronic contributions to the reaction field that is necessary in the Franck-Condon state, the energy of the chromophore in the excited state is

$$W_e^{FC} = \frac{1}{2}\mathbf{m}_g \cdot \mathbf{R}_g^{or} + \frac{1}{2}\mathbf{m}_e \cdot \mathbf{R}_e^{el} - \mathbf{p}_e \cdot \mathbf{R}_e^{FC} - \frac{1}{2}\alpha_e |\mathbf{R}_e^{FC}|^2. \tag{14}$$

All reaction fields, $\mathbf{R}$, and total dipole moments, $\mathbf{m}$, that appear in Eq. 14 were specified in the previous subsection (with the exception of $\mathbf{R}_e^{el} = f'\mathbf{m}_e$). After some algebra, the final result is

$$W_e^{FC} = -\frac{1}{2}\frac{1}{1-\alpha_e f'}\left(f'|\mathbf{p}_e|^2 + \frac{2(f-f')}{1-\alpha_g f}\mathbf{p}_e \cdot \mathbf{p}_g - \frac{1-\alpha_e f}{(1-\alpha_g f)^2}(f-f')|\mathbf{p}_g|^2\right). \tag{15}$$

Simplifications ensue if it is assumed that the polarizabilities are the same in ground and excited states, i.e., $\alpha_g = \alpha_e (\equiv \alpha)$. In practice, this approximation is generally made when analyzing experimental data (25,26).

The shift in wavenumber of the absorption band, $\Delta\bar{\nu}_a$, that is induced by the solvent is given by the difference in perturbations of the chromophore energy in the ground and Franck-Condon excited states,

$$hc\Delta\bar{\nu}_a = W_e^{FC} - W_g, \tag{16}$$

where h is Planck's constant and c is the velocity of light in vacuo. From Eqs. 6 and 15, the shift in absorption maximum is given by

$$hc\Delta\overline{\nu}_{\mathrm{a}} = -\left(\frac{f}{1-\alpha f}-\frac{f'}{1-\alpha f'}\right)(\mathbf{p}_{\mathrm{e}}-\mathbf{p}_{\mathrm{g}})\cdot\mathbf{p}_{\mathrm{g}} - \frac{1}{2}\frac{f'}{1-\alpha f'}\left(|\mathbf{p}_{\mathrm{e}}|^2-|\mathbf{p}_{\mathrm{g}}|^2\right), \quad (17)$$

where polarizabilities in the ground and excited states are assumed to be equal. This differs from the corresponding expression derived by Bilot and Kawski (24) because the work done in changing the polarization of the dielectric was neglected in the latter work. Consideration of the dispersion interactions between the chromophore and the surrounding solvent molecules adds a further term $-f'D$ to the shift in absorption maximum, where D is a positive constant for a given low-lying electronic excitation (25). Hence, the total dependence of the shift in absorption maximum on solvent dielectric constant and refractive index is

$$hc\Delta\overline{\nu}_{\mathrm{a}} = -\left(\frac{f(\varepsilon_{\mathrm{r}})}{1-\frac{\alpha}{4\pi\varepsilon_{\mathrm{o}}r_{\mathrm{eff}}^3}f(\varepsilon_{\mathrm{r}})}-\frac{f(n^2)}{1-\frac{\alpha}{4\pi\varepsilon_{\mathrm{o}}r_{\mathrm{eff}}^3}f(n^2)}\right)\times\frac{(\mathbf{p}_{\mathrm{e}}-\mathbf{p}_{\mathrm{g}})\cdot\mathbf{p}_{\mathrm{g}}}{4\pi\varepsilon_{\mathrm{o}}r_{\mathrm{eff}}^3} - \frac{1}{2}\frac{f(n^2)}{1-\frac{\alpha}{4\pi\varepsilon_{\mathrm{o}}r_{\mathrm{eff}}^3}f(n^2)}\times\frac{\left(|\mathbf{p}_{\mathrm{e}}|^2-|\mathbf{p}_{\mathrm{g}}|^2\right)}{4\pi\varepsilon_{\mathrm{o}}r_{\mathrm{eff}}^3} - Df(n^2), \quad (18)$$

where the substitutions in Eqs. 2 and 8 are made explicitly. The form of the function $f(\varepsilon_{\mathrm{r}})$ or $f(n^2)$ depends on the model used to determine the reaction field.

Fluorescence spectrum and Stokes shift

Because the dielectric relaxation time (τ_{D}) is considerably shorter than the fluorescence lifetime (τ_{f}), the solvent dipoles reorient to their equilibrium situation in the excited state before emission of the radiation. Therefore, the fluorescence emission takes place from the equilibrium excited state to the Franck-Condon ground state (see Fig. 2). By reasoning similar to that giving rise to Eq. 17, the solvent-dependent shift in the fluorescence maximum is then given by (25)

$$hc\Delta\overline{\nu}_{\mathrm{f}} = -\left(\frac{f}{1-\alpha f}-\frac{f'}{1-\alpha f'}\right)(\mathbf{p}_{\mathrm{e}}-\mathbf{p}_{\mathrm{g}})\cdot\mathbf{p}_{\mathrm{e}} - \frac{1}{2}\frac{f'}{1-\alpha f'}\left(|\mathbf{p}_{\mathrm{e}}|^2-|\mathbf{p}_{\mathrm{g}}|^2\right) - Df' \quad (19)$$

for $\tau_{\mathrm{D}} << \tau_{\mathrm{f}}$. Expressed explicitly in terms of the solvent properties, this becomes

$$hc\Delta\overline{\nu}_{\mathrm{f}} = -\left(\frac{f(\varepsilon_{\mathrm{r}})}{1-\frac{\alpha}{4\pi\varepsilon_{\mathrm{o}}r_{\mathrm{eff}}^3}f(\varepsilon_{\mathrm{r}})}-\frac{f(n^2)}{1-\frac{\alpha}{4\pi\varepsilon_{\mathrm{o}}r_{\mathrm{eff}}^3}f(n^2)}\right)\times\frac{(\mathbf{p}_{\mathrm{e}}-\mathbf{p}_{\mathrm{g}})\cdot\mathbf{p}_{\mathrm{e}}}{4\pi\varepsilon_{\mathrm{o}}r_{\mathrm{eff}}^3} - \frac{1}{2}\frac{f(n^2)}{1-\frac{\alpha}{4\pi\varepsilon_{\mathrm{o}}r_{\mathrm{eff}}^3}f(n^2)}\times\frac{\left(|\mathbf{p}_{\mathrm{e}}|^2-|\mathbf{p}_{\mathrm{g}}|^2\right)}{4\pi\varepsilon_{\mathrm{o}}r_{\mathrm{eff}}^3} - Df(n^2). \quad (20)$$

From Eqs. 18 and 20, the difference in wavenumber of the fluorescence and absorption maxima, i.e., the Stokes shift ($\Delta\overline{\nu}_{\mathrm{Stokes}}$), is given by

$$hc\Delta\overline{\nu}_{\mathrm{Stokes}} \equiv hc\left(\Delta\overline{\nu}_{\mathrm{a}}-\Delta\overline{\nu}_{\mathrm{f}}\right) = \left(\frac{f(\varepsilon_{\mathrm{r}})}{1-\frac{\alpha}{4\pi\varepsilon_{\mathrm{o}}r_{\mathrm{eff}}^3}f(\varepsilon_{\mathrm{r}})}-\frac{f(n^2)}{1-\frac{\alpha}{4\pi\varepsilon_{\mathrm{o}}r_{\mathrm{eff}}^3}f(n^2)}\right)\frac{|\mathbf{p}_{\mathrm{e}}-\mathbf{p}_{\mathrm{g}}|^2}{4\pi\varepsilon_{\mathrm{o}}r_{\mathrm{eff}}^3}. \quad (21)$$

Correspondingly, the shift in the sum of the absorption and emission frequencies ($\sum\overline{\nu}$) is given by

$$hc\sum\overline{\nu} = hc\left(\Delta\overline{\nu}_{\mathrm{a}}+\Delta\overline{\nu}_{\mathrm{f}}\right) = -\frac{f(\varepsilon_{\mathrm{r}})}{1-\frac{\alpha}{4\pi\varepsilon_{\mathrm{o}}r_{\mathrm{eff}}^3}f(\varepsilon_{\mathrm{r}})}\frac{\left(|\mathbf{p}_{\mathrm{e}}|^2-|\mathbf{p}_{\mathrm{g}}|^2\right)}{4\pi\varepsilon_{\mathrm{o}}r_{\mathrm{eff}}^3} - 2Df(n^2), \quad (22)$$

which, unlike the Stokes shift, depends on the energy of the dispersion interaction. Expressions corresponding to Eqs. 21 and 22, but for $\alpha_{\mathrm{e}} - \alpha_{\mathrm{g}} \neq 0$ and for anisotropic polarizabilities are given by Liptay (25). Equation 21 differs from the original Lippert equation in that the polarizability α of the fluorophore is taken into account. As pointed out originally by Liptay (25), other attempts to do this (22–24,26,30) have led to incorrect results.

MODELS FOR REACTION FIELDS

The various models for the reaction field are characterized by the function $f(\varepsilon_{\mathrm{r}})$ (see Eqs. 2 and 8). The Onsager model for the reaction field involves a step-function transition from the dielectric permittivity of free space, ε_{o}, to that of the bulk solvent, $\varepsilon_{\mathrm{o}}\varepsilon_{\mathrm{r}}$, at the radial distance r_{eff} (see Fig. 3). The corresponding expression for the dependence of the reaction field on the relative dielectric permittivity ε_{r}, which is obtained from the solution of Laplace's equation, is (31)

$$f_{\mathrm{o}}(\varepsilon_{\mathrm{r}}) = \frac{2(\varepsilon_{\mathrm{r}}-1)}{2\varepsilon_{\mathrm{r}}+1}. \quad (23)$$

Together with Eqs. 2 and 3, this gives Onsager's result for the strength of the reaction field.

Subsequently, Block and Walker (28) proposed a more gradual transition to the bulk dielectric permittivity. This has a radial dependence given by: $\varepsilon_{\mathrm{r}}(r) = \varepsilon_{\mathrm{B}}\exp(-\kappa/r)$, where the exponential decay constant, κ, is determined by the boundary condition $\varepsilon_{\mathrm{r}} = 1$ at $r = r_{\mathrm{eff}}$ (see Fig. 3). An

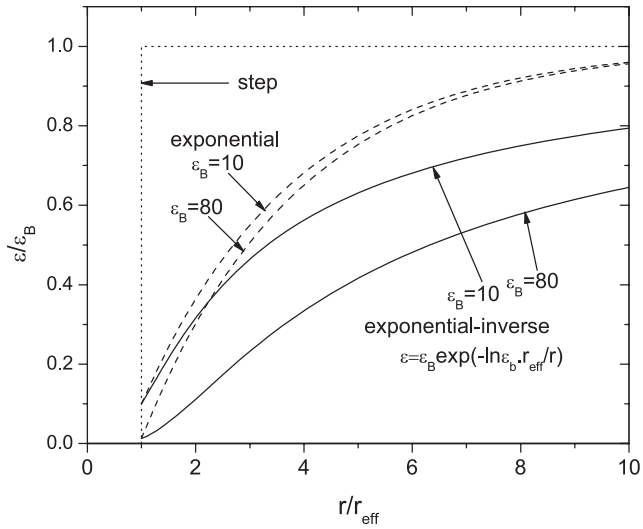

FIGURE 3 Radial dependence of the relative dielectric permittivity for different models of the reaction field. (*Dotted line*) Step function, from Onsager (31). (*Solid line*) Exponential-inverse transition, from Block and Walker (28). (*Dashed line*) Direct exponential transition, from Ehrenson (16). r_{eff} is the effective molecular radius of the chromophore. The starting level is $\varepsilon_r = 1$, for $r/r_{eff} \leq 1$.

analytical solution of Laplace's equation is possible for this form of $\varepsilon_r(r)$ and yields

$$f_{BW}(\varepsilon_r) = \frac{3\varepsilon_r \ln \varepsilon_r}{\varepsilon_r \ln \varepsilon_r - \varepsilon_r + 1} - \frac{6}{\ln \varepsilon_r} - 2 \qquad (24)$$

for the dependence on ε_r in Eq. 2.

The exponential-inverse radial dependence suggested by Block and Walker (28) reaches the bulk dielectric constant only at large distances. Ehrenson (15,16) has proposed, instead, a direct exponential transition, $\varepsilon_r(r) = \varepsilon_B - (\varepsilon_B - 1)2^{-(r-r_{eff})/2r_{eff}}$, which reaches half the bulk dielectric constant at radial distance $r = 3r_{eff}$ (see Fig. 3). Numerical solutions of Laplace's equation are necessary for this functional form. The solution obtained by Ehrenson (15,16) using a shell model can be fit approximately with the polynomial

$$f_E(\varepsilon_r) = 6.313 \times 10^{-2} \times \left[1 + 1.058 \ln \varepsilon_r - 0.190(\ln \varepsilon_r)^2 + 0.009(\ln \varepsilon_r)^3\right] \ln \varepsilon_r. \qquad (25)$$

This expression can be used in nonlinear least-squares fitting of experimental data.

A statistical mechanical approach to analyzing dielectric permittivity, which can be cast in the reaction-field formalism, has been given by Wertheim (33). Originally developed for nonpolar fluids, the model uses the mean spherical approximation (MSA) and has subsequently been extended to a polarizable hard-sphere fluid with permanent dipoles (34). This MSA approach gives the following parametric expression for the relative dielectric permittivity (33,34)

$$\varepsilon_r = \frac{(1 + 4\xi)^2(1 + \xi)^4}{(1 - 2\xi)^6}. \qquad (26)$$

The corresponding parametric expression for the reaction field strength is (14,27)

$$f_W(\varepsilon_r) = 16\xi. \qquad (27)$$

Together with Eqs. 2 and 3, Eqs. 26 and 27 give the dependence of the reaction-field strength on ε_r. Over the range ε_r = 1–200, combination of Eqs. 26 and 27 may be approximated by the polynomial

$$f_W(\varepsilon_r) \approx 0.6666 \times \left[1 + 0.0171 \ln \varepsilon_r - 0.00432(\ln \varepsilon_r)^2 + 0.000158(\ln \varepsilon)^3\right] \ln \varepsilon_r. \qquad (28)$$

Fig. 4 shows the function $f(\varepsilon_r)/(1-af(\varepsilon_r))$ in the different models for the reaction field, with different values of the polarizability of the chromophore. Neglecting the polarizability is given by $a = 0$ (*dotted lines*). In general, the polarizability is given in terms of the Lorenz-Lorentz relation: $a \equiv \alpha^2/4\pi\varepsilon_o r_{eff}^3 = (n_o^2-1)/(n_o^2+2)$, where n_o is the refractive index of the chromophore extrapolated to zero frequency. A value of $a = 1/4$ (*dashed lines*) is appropriate to the refractive index of nitroxide spin labels (27) and a value of $a = 1/2$ (*solid lines*) has been suggested for fluorophores (21–23,26).

As is well known, the Onsager reaction field, with a stepwise transition in dielectric constant, saturates rapidly with

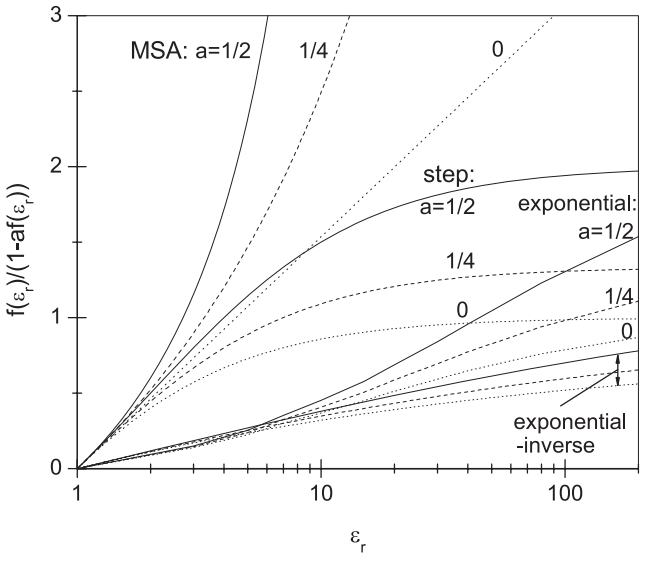

FIGURE 4 Dependence of the strength of the reaction field, $f(\varepsilon_r)/(1-af(\varepsilon_r))$, on the dielectric constant, ε_r (or refractive index), in different models. Reaction fields are depicted for a step transition to the bulk dielectric constant (31), a direct exponential dependence on radial distance (16), an exponential dependence on inverse radial distance (28), or for a hard-sphere model in the MSA (33,34), as indicated. Reaction fields are computed for different polarizabilities, α, of the chromophore: $a \equiv \alpha^2/(4\pi\varepsilon_o r_{eff}^3) = 0$ (*dotted line*), 1/4 (*dashed lined*), or 1/2 (*solid line*). The abscissa has a logarithmic scale.

increasing dielectric permittivity. The direct exponential transition in dielectric permittivity of references (15,16) extends out to ~2–3 shells, and therefore the reaction field saturates less rapidly than does that of Onsager. The reaction field of Block and Walker (28), which is characterized by a broader transition in dielectric permittivity, saturates least rapidly. On the other hand, reaction fields predicted by the model with mean spherical approximation of Wertheim (33,34) increase far more steeply with increasing dielectric permittivity than any of the three continuum models, and do not reach saturation. For all models, increasing polarizability of the chromophore increases the strength of the reaction field.

For the continuum-dielectric models, the function $f(\varepsilon_r)$ tends to a limiting value with increasing ε_r of $f(\infty) \rightarrow 1$. Allowing for polarizability of the chromophore, the function $f(\varepsilon_r)/(1-af(\varepsilon_r))$ therefore tends to a limiting value of $1/(1-a)$. For the MSA model, the limiting value is much larger: $f(\infty) = 8$, and hence $f(\varepsilon_r)/(1-af(\varepsilon_r))$ tends to diverge with increasing dielectric permittivity.

APPLICATIONS

Fig. 5 gives the dependence of the Stokes shift on relative dielectric permittivity of the solvent for three different fluorophore types that have been used for polarity studies in biological systems. The experimental data are indicated by squares. Hydrogen-bonding solvents (*open squares*) are clearly distinguished from those without a proton donor (*solid squares*), in the case of the fluorophores with a carbonyl H-bond acceptor [i.e., PRODAN (2-(dimethylamino)-6-propionyl-naphthalene), and 8-AS (methyl 8-(2-anthroyl)octanoate)].

For the aprotic solvents, nonlinear least-squares fitting, with the dependence of the Stokes shift on ε_r and n that is predicted in Eq. 21 for the different models of the reaction field (Eqs. 23–25 and 28), is given by the lines and small symbols in Fig. 5. (Note that the lines simply join the points in Fig. 5. They do not indicate a functional dependence on dielectric permittivity, because the fitting with Eq. 21 additionally involves the dependence on refractive index.) For PRODAN, which contains the same chromophore as LAURDAN (2-(dimethylamino)-6-lauroyl-naphthalene), best fitting is obtained with the Block-Walker model (*solid line*) for the reaction field ($r = 0.994$), although that with the Ehrenson model (*dashed* and *dotted line*) is almost equally good. Including polarizability of the fluorophore improves the quality of the fit. For the Block-Walker model with PRODAN, optimization yields $n_o^2 = 2.73$. For the anthroxy fatty acid, 8-AS, the Wertheim model of the reaction field (*dashed line*) gives the best fit ($r = 0.953$), with that of Ehrenson (*dashed* and *dotted line*), and of Block and Walker (*solid line*), being somewhat less good. Again, inclusion of fluorophore polarizability improves the fit, with an optimized value of $n_o^2 = 2.22$ for 8-AS with the Wertheim reaction field. For DANSAEP [*N*-(2-(((5-(*N*,*N*-dimethylamino)-1-naphthalenyl)sulphonyl)-amino)ethyl)-2-propenamide], the Onsager model (*dotted line*) yields the best fit ($r = 0.989$), with the reaction field of Block and Walker (*solid line*) giving a close second-best fit. Again, using a nonzero polarizability for DANSAEP improves the fit, with an optimized value of $n_o^2 = 2.23$ for DANSAEP with the Onsager reaction field.

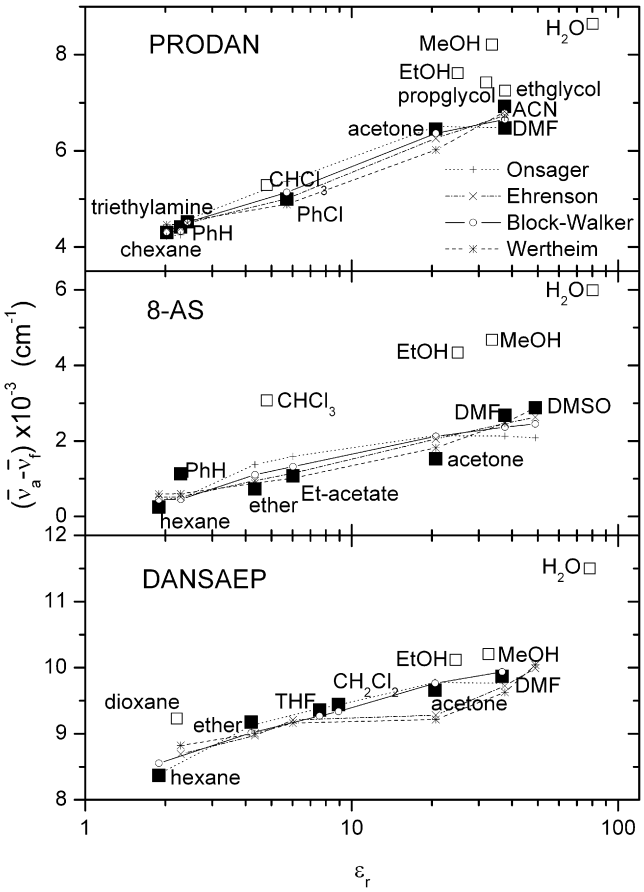

FIGURE 5 Stokes shifts, $\bar{\nu}_a - \bar{\nu}_f$ (*squares*), for the fluorophores PRODAN (45), 8-AS (7), and DANSAEP (46), as function of relative dielectric permittivity, ε_r, of the solvent. Fitting the data for aprotic solvents (*solid squares*) by Eq. 21, expressed as $\bar{\nu}_a - \bar{\nu}_f = K_f[f(\varepsilon_r)/(1-af(\varepsilon_r)) - f(n^2)/(1-af(n^2))] + \Delta\bar{\nu}_o$, is given for the different models of the reaction field: Onsager (Eq. 23, *dotted lines*), Ehrenson (Eq. 25, *dashed* and *dotted lines*), Block-Walker (Eq. 24, *solid lines*), and Wertheim (Eq. 28, *dashed lines*). The abscissa has a logarithmic scale. (*Open squares* are for protic solvents.)

There is, therefore, some experimental variation regarding what constitutes the optimum reaction field for fitting the polarity dependence of the various fluorophores. However, the reaction-field of Block and Walker (28) provides either the best or close to second-best description of the solvatochromism. Therefore, this can best be used for a consistent comparison between different fluorophores. A further reason for choosing the Block-Walker model is that this best describes the polarity dependence of nitroxide spin labels (27). As already mentioned, spin-label EPR measurements involve only the ground state and therefore constitute a simpler and more direct test of the different models. Finally,

choice of the Block-Walker model also allows a consistent comparison between fluorescent probes and spin-label probes. Note that the spin-label EPR results clearly indicate that the Block-Walker model is most appropriate, and therefore slight deviations from this in the present case can be attributed to uncertainties arising from the added complexities in the fluorescence experiment.

Fig. 6 shows the dependence of the Stokes shift on the modified Lippert parameter (see Eq. 21): $f_{BW}(\varepsilon_r)/(1-af_{BW}(\varepsilon_r)) - f_{BW}(n^2)/(1-af_{BW}(n^2))$ that is defined in terms of the Block-Walker reaction field, with allowance for polarizability of the fluorophore. A value of $a = 1/4$ is chosen, corresponding to ${n_o}^2 = 2$, because this is close to the optimized values obtained in the nonlinear fits. (In practice, small deviations from ${n_o}^2 = 2$ provide only small improvements in the quality of the fit.) The fitting parameters K_f and $\Delta\nu_o$ that are obtained from the linear regressions for aprotic solvents in Fig. 6 (excluding dioxane and benzene) are listed in Table 1.

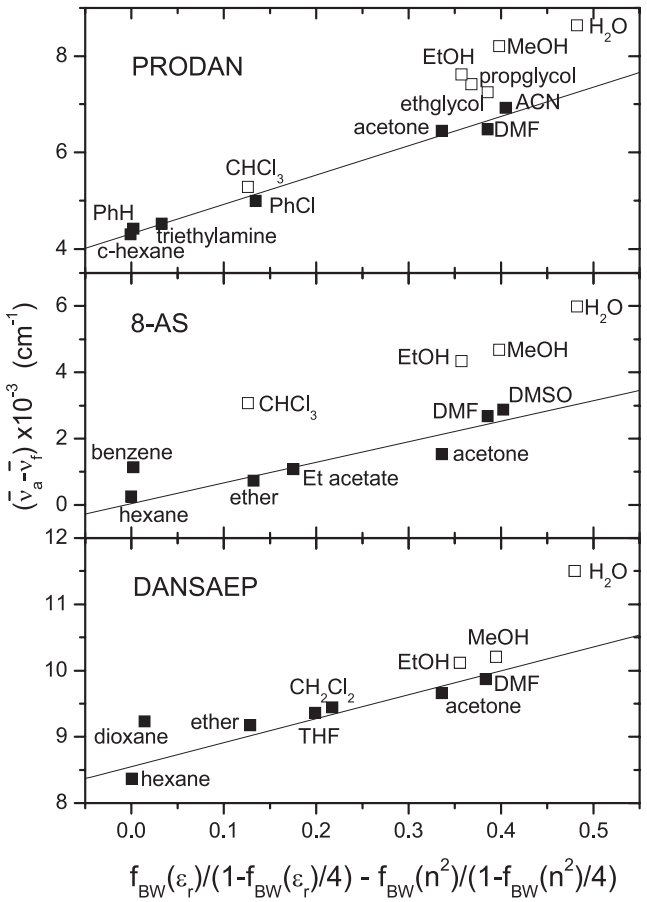

FIGURE 6 Dependence of the Stokes shift for PRODAN (45), 8-AS (7), and DANSAEP (46) on the parameter $f_{BW}(\varepsilon_r)/(1-f_{BW}(\varepsilon_r)/4) - f_{BW}(n^2)/(1-f_{BW}(n^2)/4)$, where the strength of the Block-Walker reaction field $f_{BW}(\ldots)$ is given by Eq. 24, and ε_r and n are the relative dielectric permittivity and refractive index of the solvent. Solid lines are linear regressions to the data for aprotic solvents (*solid squares*). (*Open squares* are for protic solvents.)

TABLE 1 Fitting parameters for the polarity dependence of the Stokes shift: $\bar{\nu}_a - \bar{\nu}_f = K_f[f_{BW}(\varepsilon_r)/(1-f_{BW}(\varepsilon_r)/4) - f_{BW}(n^2)/(1-f_{BW}(n^2)/4)] + \Delta\bar{\nu}_o$ for different fluorophores (see Fig. 6)

Probe	K_f (cm^{-1})	$\Delta\bar{\nu}_o$ (cm^{-1})
PRODAN	6083 ± 298	4315 ± 75
8-AS	6214 ± 1073	39 ± 301
DANSAEP	3611 ± 497	8551 ± 122

INTERCOMPARISONS AND CALIBRATIONS

The parameters in Table 1 for aprotic media allow definition of the Stokes shifts from different fluorophores that correspond to the same value of the reaction field, i.e., to the same environmental polarity. For fluorophores 1 and 2, the respective Stokes shifts are related by

$$\left(\bar{\nu}_a - \bar{\nu}_f\right)_1 = \frac{K_{f,1}}{K_{f,2}}\left(\bar{\nu}_a - \bar{\nu}_f\right)_2 + \Delta\bar{\nu}_{o,1} - \frac{K_{f,1}}{K_{f,2}}\Delta\bar{\nu}_{o,2}, \qquad (29)$$

where $K_{f,1}$, $K_{f,2}$ and $\Delta\bar{\nu}_{o,1}$, $\Delta\bar{\nu}_{o,2}$ are the values of K_f and $\Delta\bar{\nu}_o$ for fluorophore 1 and fluorophore 2, respectively. For example, the gradient and intercept parameters for these calibrations are $K_{f,1}/K_{f,2} = 1.0, 0.59$ and $\Delta\bar{\nu}_{o,1} - (K_{f,1}/K_{f,2})\Delta\bar{\nu}_{o,2} = -4370, 5990$ cm^{-1} for 8-AS and DANSAEP, respectively, when referring the Stokes shifts of these fluorophores to those of PRODAN.

A somewhat more complicated situation arises in the comparison of Stokes shifts with the hyperfine couplings of nitroxide spin labels, which are used to determine transmembrane polarity profiles in lipid bilayer membranes (1,35). This is because the polarity sensitivity of spin-label hyperfine couplings depends only on the reaction field in the equilibrium ground state. The isotropic ^{14}N-hyperfine coupling of a nitroxide is given by (13,27)

$$a_o^N = K_\nu \frac{f_{BW}(\varepsilon_r)}{1 - \frac{1}{4}f_{BW}(\varepsilon_r)} + a_o^{\varepsilon=1}, \qquad (30)$$

where K_ν is a calibration constant and $a_o^{\varepsilon=1}$ is the hyperfine coupling in a medium with $\varepsilon_r = 1$. The fluorophore Stokes shift is thus related to the spin-label hyperfine coupling by

$$\left(\bar{\nu}_a - \bar{\nu}_f\right) = \frac{K_f}{K_\nu}\left(a_o^N - a_o^{\varepsilon=1}\right) + \Delta\bar{\nu}_o - K_f\frac{f_{BW}(n^2)}{1 - \frac{1}{4}f_{BW}(n^2)}, \qquad (31)$$

where the term involving the refractive index of the medium remains because the EPR spectrum does not involve Franck-Condon states. Fortunately, the variation in n^2 is much less than that in the dielectric constant, ε_r. For the range of aprotic solvents represented in Fig. 6, the mean value of $f_{BW}(n^2)/(1-f_{BW}(n^2)/4)$ is 0.113 with a standard deviation of 0.012 ($N = 14$). For the protic solvents, the corresponding value is 0.107 ± 0.013 ($N = 6$). Thus, for aprotic environments, it is reasonable to approximate the final term on the right in Eq. 31 by 0.11 × K_f, when establishing the correlation between fluorophore and spin-label measurements.

For DOXYL spin-labeled lipid chains, the calibration parameters in aprotic media are $K_v = 0.087 \pm 0.012$ mT and $a_o^{\varepsilon=1} = 1.410 \pm 0.005$ mT (36); values for other nitroxide spin labels are given in references (27,36). As an example of the application of Eq. 31, the isotropic hyperfine couplings of spin-labeled lipid chains in the center of fluid phospholipid bilayers have plateau values in the range $a_o^N = 1.440-1.455$ mT in the absence of cholesterol (L_α phase), and $a_o^N = 1.423-1.433$ mT in the presence of 50 mol % cholesterol (L_o phase) (1). These correspond to Stokes shifts of $\Delta\bar{\nu}_{Stokes} = 5725-6775$ and $4540-5235$ cm^{-1}, respectively, for PRODAN; $1480-2550$ and $265-980$ cm^{-1}, respectively, for 8-AS; and $9390-10010$ and $8685-9100$ cm^{-1}, respectively, for DANSAEP. For comparison, the phosphatidylcholine variant of 8-AS has Stokes shifts of $\Delta\bar{\nu}_{Stokes} = 3448$ and 2169 cm^{-1} in fluid egg phosphatidylcholine (PC) membranes without and with 50 mol % cholesterol, respectively (37). These correspond to environments with polarities that are considerably greater than at the hydrophobic center of the membranes.

As for spin-label hyperfine couplings (36), the Stokes shifts of 8-AS and PRODAN in the hydrogen-bonding alcohol solvents depend approximately linearly on the molar concentration, [OH], of hydroxyl groups. Values of gradient $\partial\Delta\bar{\nu}_{Stokes}/\partial[OH] = 42.8 \pm 0.3$ and 27 ± 8 cm^{-1} M^{-1}, and of intercept $\Delta\bar{\nu}_{Stokes,o} = 3611 \pm 11$ and 7225 ± 260 cm^{-1}, are obtained for 8-AS and PRODAN, respectively. For spin-labeled lipid chains, the corresponding gradient is $\partial a_o^N/\partial[OH] = 0.0023 \pm 0.0001$ mT M^{-1} and intercept $a_{o,o}^N = 1.449 \pm 0.003$ mT. By using this approximation, the fluorophore Stokes shift is related to the spin-label hyperfine coupling simply by

$$\Delta\bar{\nu}_{Stokes} = \left(\frac{\partial\Delta\bar{\nu}_{Stokes}/\partial[OH]}{\partial a_o^N/\partial[OH]}\right)\left(a_o^N - a_{o,o}^N\right) + \Delta\bar{\nu}_{Stokes,o}. \quad (32)$$

As an example of the application of Eq. 32, the isotropic hyperfine couplings of spin-labels at the polar-group ends of the lipid chains in fluid phospholipid bilayers have plateau values in the range $a_o^N = 1.497-1.527$ mT in the absence of cholesterol (L_α phase), and $a_o^N = 1.510-1.527$ mT in the presence of 50 mol % cholesterol (L_o phase) (1). These correspond to Stokes shifts of $\Delta\bar{\nu}_{Stokes} = 4505-5065$ and $4745-5065$ cm^{-1}, respectively, for 8-AS; and $7785-8135$ and $7940-8135$ cm^{-1}, respectively, for PRODAN. For 8-AS, these upper plateau values are considerably higher than those for the phosphatidylcholine derivative in phospholipid vesicles ((37), and see above).

Finally, the Stokes shifts of the fluorophores may be related to the transmembrane polarity profile of phospholipid bilayers. The latter has been determined at high positional resolution by using glycerophospholipids spin-labeled systematically in the *sn*-2 chain (1). It is found that the positional dependence of the isotropic hyperfine couplings can be described to high accuracy by a Boltzmann sigmoidal form. The same is true of the water distribution determined by D_2O-ESEEM spectroscopy (38), the oxygen and nitric oxide distributions determined by nonlinear EPR (39–41), and the polarity-dependent spin-label g_{xx}-values determined by high-field EPR (42). In terms of the Stokes shifts of fluorophores, the polarity profile may therefore be expressed relative to the C-atom positions, n_c, in the phospholipid chain as

$$\Delta\bar{\nu}_{Stokes}(n_c) = \frac{\Delta\bar{\nu}_{Stokes,1} - \Delta\bar{\nu}_{Stokes,2}}{1 + \exp((n_c - n_{c,o})/\lambda)} + \Delta\bar{\nu}_{Stokes,2}, \quad (33)$$

where $\Delta\bar{\nu}_{Stokes,1}$ and $\Delta\bar{\nu}_{Stokes,2}$ are the limiting values of $\Delta\bar{\nu}_{Stokes}$ in the region of the polar headgroup and terminal methyl ends of the lipid chain, respectively, and λ is a decay constant (see also (43)). This dependence on intramembrane location has been verified experimentally for the Stokes shifts of the M13 coat protein, which was site-specifically labeled with AEDANS (9).

Fig. 7 shows the predicted dependence on transmembrane location of the Stokes shift for the anthroyl (8-AS) or PRODAN chromophores in fluid-phase membranes of dipalmitoyl phosphatidylcholine (DPPC) with and without 50 mol % cholesterol. These profiles are based on the parameters $n_{c,o}$ and λ characterizing the shape of the profile in Eq. 33 that are determined from EPR experiments with spin-labeled lipid chains (1). Correspondences with EPR hyperfine couplings that are based on Eq. 31 are used to determine

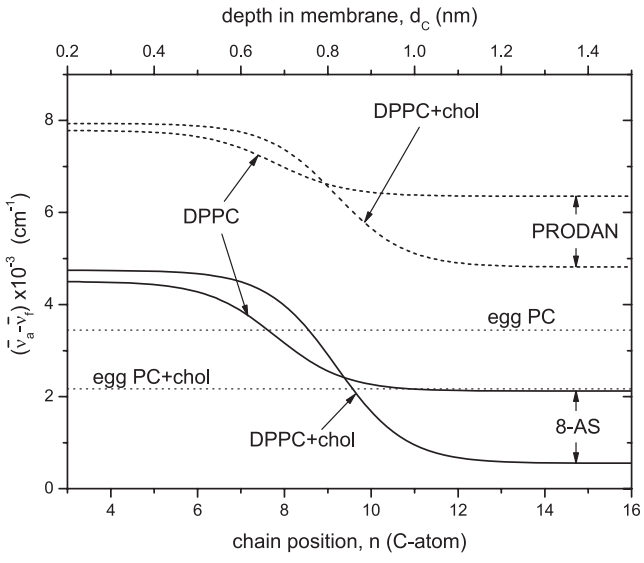

FIGURE 7 Predicted dependence of the Stokes shift for the fluorophore of 8-AS and PRODAN on depth in fluid DPPC or DPPC + 50 mol % cholesterol (chol) bilayer membranes. The profile is deduced from spin labels at positions n_c in the *sn*-2 chain of phosphatidylcholine (1), together with correlations between fluorophore Stokes shift and spin-label hyperfine splitting. (*Horizontal dotted lines*) Experimental values for the PC derivative of 8-AS in vesicles of egg PC and egg PC + 50 mol % cholesterol (37). The upper abscissa gives the estimated distance, d_C, from the lipid chain carbonyl group ($n_c = 1$).

the values for $\Delta\overline{\nu}_{\mathrm{Stokes},2}$ and those based on Eq. 32 are used to determine the values for $\Delta\overline{\nu}_{\mathrm{Stokes},1}$, from the EPR-determined values of $a^{\mathrm{N}}_{\mathrm{o},2}$ and $a^{\mathrm{N}}_{\mathrm{o},1}$, respectively, that are given in Marsh (1) (and see above). Different EPR-fluorescence correlations are used in the two regions because polarity-induced shifts are determined mostly by dielectric polarization in the predominantly aprotic environment at the membrane midplane (i.e., region 2), whereas they are dominated by hydrogen bonding of water in the protic environment at the top of the chains (i.e., region 1). The Stokes shifts for PC with an 8-(2-anthroyl)octanoyl *sn*-2 chain in fluid lipid vesicles are indicated in Fig. 7 (*horizontal dotted lines*). In egg PC alone this corresponds with the calibration for the $n_{\mathrm{c}} = 8$ position, consistent with the point of attachment of the anthroyl chromophore to the lipid chain. In egg PC + 50 mol % cholesterol, the smaller Stokes shift correlates with the $n_{\mathrm{c}} = 9-10$ position, corresponding to an ordering of the anthroyl moiety toward the membrane midplane by cholesterol. These results indicate the general utility of calibrations such as those constructed in Fig. 7 for determining the location of fluorophores in biological membranes; cf. for instance, Marsh et al. (44).

REFERENCES

1. Marsh, D. 2001. Polarity and permeation profiles in lipid membranes. *Proc. Natl. Acad. Sci. USA*. 98:7777–7782.
2. Griffith, O. H., P. J. Dehlinger, and S. P. Van. 1974. Shape of the hydrophobic barrier of phospholipid bilayers. Evidence for water penetration in biological membranes. *J. Membr. Biol.* 15:159–192.
3. Subczynski, W. K., A. Wisniewska, J. J. Yin, J. S. Hyde, and A. Kusumi. 1994. Hydrophobic barriers of lipid bilayer membranes formed by reduction of water penetration by alkyl chain unsaturation and cholesterol. *Biochemistry*. 33:7670–7681.
4. Fretten, P., S. J. Morris, A. Watts, and D. Marsh. 1980. Lipid-lipid and lipid-protein interactions in chromaffin granule membranes. *Biochim. Biophys. Acta*. 598:247–259.
5. Pates, R. D., and D. Marsh. 1987. Lipid mobility and order in bovine rod outer segment disk membranes. A spin-label study of lipid-protein interactions. *Biochemistry*. 26:29–39.
6. Thulborn, K. R., L. M. Tilley, W. H. Sawyer, and F. E. Treloar. 1979. The use of *n*-(9-anthroyloxy) fatty acids to determine fluidity and polarity gradients in phospholipid bilayers. *Biochim. Biophys. Acta*. 558:166–178.
7. Perochon, E., A. Lopez, and J. F. Tocanne. 1991. Fluorescence properties of methyl 8-(2-anthroyl) octanoate, a solvatochromic lipophilic probe. *Chem. Phys. Lipids*. 59:17–28.
8. Parasassi, T., E. K. Krasnowska, L. Bagatolli, and E. Gratton. 1998. LAURDAN and PRODAN as polarity-sensitive fluorescent membrane probes. *J. Fluoresc*. 8:365–373.
9. Koehorst, R. B. M., R. B. Spruijt, F. J. Vergeldt, and M. A. Hemminga. 2004. Lipid bilayer topology of the transmembrane α-helix of M13 major coat protein and bilayer polarity profile by site-directed fluorescence spectroscopy. *Biophys. J*. 87:1445–1455.
10. Carney, J., J. M. East, and A. G. Lee. 2007. Penetration of lipid chains into transmembrane surfaces of membrane proteins: studies with MscL. *Biophys. J*. 92:3556–3563.
11. Abboud, J. -L. M., and R. W. Taft. 1979. An interpretation of a general scale of solvent polarities. A simplified reaction field theory modification. *J. Phys. Chem*. 83:412–419.
12. Mukerjee, P., C. Ramachandran, and R. A. Pyter. 1982. Solvent effects on the visible spectra of nitroxides and relation to nitrogen hyperfine splitting constants. Nonempirical polarity scales for aprotic and hydroxylic solvents. *J. Phys. Chem*. 86:3189–3197.
13. Marsh, D. 2002. Polarity contributions to hyperfine splittings of hydrogen-bonded nitroxides—the microenvironment of spin labels. *J. Magn. Reson*. 157:114–118.
14. Reddoch, A. H., and S. Konishi. 1979. The solvent effect on di-*tert*-butyl nitroxide. A dipole-dipole model for polar solutes in polar solvents. *J. Chem. Phys*. 70:2121–2130.
15. Ehrenson, S. 1981. Cavity boundary effects within the Onsager theory for dielectrics. *J. Comput. Chem*. 2:41–52.
16. Ehrenson, S. 1981. Classical electrical contributions to solvent polarity scales. *J. Am. Chem. Soc*. 103:6036–6043.
17. Abe, T., S. Tero-Kubota, and Y. Ikegami. 1982. Theory of solvent effects on the hyperfine splitting constants in ESR spectra of free radicals. *J. Phys. Chem*. 86:1358–1365.
18. Ottaviani, M. F., G. Martini, and L. Nuti. 1987. Nitrogen hyperfine splitting constant of nitroxide solutions: differently structured and charged nitroxides as probes of environmental properties. *Magn. Reson. Chem*. 25:897–904.
19. Ooshika, Y. 1954. Absorption spectra of dyes in solution. *J. Phys. Soc. Jpn*. 9:594–602.
20. Lippert, E. 1955. Dipolmoment und Elektronenstruktur von angeregten Molekülen. *Z. Naturforschg*. 10:541–545.
21. McRae, E. G. 1957. Theory of solvent effects on molecular electronic spectra. Frequency shifts. *J. Phys. Chem*. 61:562–572.
22. Bakhshiev, N. G. 1961. Universal molecular interactions and their effect on the position of the electronic spectra of molecules in two-component solutions. I. Theory (liquid solutions). *Opt. Spectrosc*. 10:379–384.
23. Bakhshiev, N. G. 1964. Universal molecular interactions and their effect on the position of the electronic spectra of molecules in two-component solutions. VII. Theory (general case of an isotropic solution). *Opt. Spectrosc*. 16:446–451.
24. Bilot, L., and A. Kawski. 1962. Zur Theorie des Einflusses von Lösungsmitteln auf die Elektronenspektren der Moleküle. *Z. Naturforschg*. 17a:621–627.
25. Liptay, W. 1965. Die Lösungsmittelabhängigkeit der Wellenzahl von Elektronenbanden und die chemisch-physikalischen Grundlagen. *Z. Naturforschg*. 20a:1441–1471.
26. Kawski, A. 2002. On the estimation of excited-state dipole moments from solvatochromic shifts of absorption and fluorescence spectra. *Z. Naturforsch*. 57a:255–262.
27. Marsh, D. 2008. Reaction fields and solvent dependence of the EPR parameters of nitroxides: the microenvironment of spin labels. *J. Magn. Reson*. 190:60–67.
28. Block, H., and S. M. Walker. 1973. Modification of Onsager theory for a dielectric. *Chem. Phys. Lett*. 19:363–364.
29. Lippert, E. 1957. Spektroskopische Bestimmung des Dipolmomentes aromatischer Verbindungen im ersten angeregten Singulettzustand. *Z. Elektrochem*. 61:962–975.
30. Lakowicz, J. R. 2006. Principles of Fluorescence Spectroscopy. Springer, New York.
31. Onsager, L. 1936. Electric moments of molecules in liquids. *J. Am. Chem. Soc*. 58:1486–1493.
32. Böttcher, C. J. F. 1973. Theory of Electric Polarization. Elsevier Scientific Publishing Company, Amsterdam.
33. Wertheim, M. S. 1973. Dielectric constant of non-polar fluids. *Mol. Phys*. 25:211–223.
34. Wertheim, M. S. 1973. Theory of polar fluids. *I. Mol. Phys*. 26:1425–1444.
35. Marsh, D. 2002. Membrane water-penetration profiles from spin labels. *Eur. Biophys. J*. 31:559–562.
36. Marsh, D., and C. Toniolo. 2008. Polarity dependence of EPR parameters for TOAC and MTSSL spin labels: correlation with DOXYL spin labels for membrane studies. *J. Magn. Reson*. 190: 211–221.

37. Perochon, E., A. Lopez, and J. F. Tocanne. 1992. Polarity of lipid bilayers—a fluorescence investigation. *Biochemistry.* 31:7672–7682.

38. Erilov, D. A., R. Bartucci, R. Guzzi, A. A. Shubin, A. G. Maryasov, et al. 2005. Water concentration profiles in membranes measured by ESEEM of spin-labeled lipids. *J. Phys. Chem. B.* 109:12003–12013.

39. Dzikovski, B. G., V. A. Livshits, and D. Marsh. 2003. Oxygen permeation profile in lipid membranes: nonlinear spin-label EPR. *Biophys. J.* 85:1005–1012.

40. Marsh, D., B. G. Dzikovski, and V. A. Livshits. 2006. Oxygen profiles in membranes. *Biophys. J.* 90:L49–L51.

41. Nedieanu, S., T. Páli, and D. Marsh. 2004. Membrane penetration of nitric oxide and its donor *S*-nitroso-*N*-acetylpenicillamine: a spin-label electron paramagnetic resonance spectroscopic study. *Biochim. Biophys. Acta.* 1661:135–143.

42. Kurad, D., G. Jeschke, and D. Marsh. 2003. Lipid membrane polarity profiles by high-field EPR. *Biophys. J.* 85:1025–1033.

43. Bartucci, R., D. A. Erilov, R. Guzzi, L. Sportelli, S. A. Dzuba, et al. 2006. Time-resolved electron spin resonance studies of spin-labeled lipids in membranes. *Chem. Phys. Lipids.* 141:142–157.

44. Marsh, D., M. Jost, C. Peggion, and C. Toniolo. 2007. Lipid chain-length dependence for incorporation of alamethicin in membranes: EPR studies on TOAC-spin labeled analogues. *Biophys. J.* 92:4002–4011.

45. Weber, G., and F. J. Farris. 1979. Synthesis and spectral properties of a hydrophobic fluorescent probe—6-propionyl-2-(dimethylamino)-naphthalene. *Biochemistry.* 18:3075–3078.

46. Ren, B., F. Gao, Z. Tong, and Y. Yan. 1999. Solvent polarity scale on the fluorescence spectra of a dansyl monomer copolymerizable in aqueous media. *Chem. Phys. Lett.* 307:55–61.